Journal of Power Sources 423 (2019) 227–235

Contents lists available at ScienceDirect

Journal of Power Sources

journal homepage: www.elsevier.com/locate/jpowsour

Improving generation ramp rates of photovoltaic systems using module-based capacitive energy storage

Bowen Zheng[a], John E. Fletcher[a], Alison Lennon[b], Yu Jiang[b], Patrick A. Burr[c,*]

[a] School of Electrical Engineering and Telecommunications, UNSW, Sydney, NSW, 2052, Australia
[b] School of Photovoltaic and Renewable Energy Engineering, UNSW, Sydney, NSW, 2052, Australia
[c] School of Mechanical and Manufacturing Engineering, UNSW, Sydney, NSW, 2052, Australia

HIGHLIGHTS

- Module-level capacitors can effectively control power ramp rates of PV systems.
- A novel ramp rate control method is reported that can optimize capacitor usage.
- Compliance to a ramp rate of ≤ 10% min^{-1} was improved from 77.9% to 94.8%.
- The proposed method was validated using 46 days of 1-s irradiance data.
- The novel control scheme is largely insensitive to model parameters.

ARTICLE INFO

Keywords:
Photovoltaics (PV)
Capacitive energy storage
Electrochemical capacitor
Ramp rate control
Module-based converter

ABSTRACT

Use of module-based capacitive energy storage devices coupled with a novel ramp rate control strategy is proposed to reduce power fluctuations of photovoltaic (PV) systems and control power ramp rate injection into the grid. The fast and dynamic response of capacitors coupled with their long cycle life can reduce the ramp rate of highly variable power output of the PV generators. Simulations based on measured 1-s irradiance data are used to verify the effectiveness of the developed method and demonstrate the reduction of generation ramp rates and increased compliance with regulatory limits achieved with the addition of the capacitive energy storage devices in individual PV modules. Our case study shows that for days with highly variable irradiance, the generation ramp rate compliance of a PV array comprising series-connected 280 W PV modules can be improved from 77.9% to 94.8% using 19.5 F capacitors rated at 41.5 V (equivalent to 16.8 kJ of energy storage) as its module-based capacitive energy storage devices. Sensitivity analyses showed that the novel control scheme was largely insensitive to the choice of the model parameters and thereby could operate robustly in the presence of variable irradiance conditions.

1. Introduction

In recent years, photovoltaics (PV) have become an increasingly important source of electrical power generation, with instantaneous penetration levels reaching 41% in South Australia in 2017 [1], residential system penetration levels above 29% in Hawaii [2] and approximately 6.7% of gross electricity consumption in Germany [3]. The increasing penetration of PV power generation poses a set of challenges to the operation of electric grids due to PV power's inherent intermittency [4–7]. The criticality of this situation is highlighted by observations that PV output power of a solar farm can be reduced by more than 66% of the rated capacity within 10 s in Alice Springs, Australia [8]. The high ramp rate of the generated power often leads to significant voltage and frequency fluctuations, causing power system instability and even collapse and blackouts. Several grid authorities are imposing limitations on maximum ramp rates: the Puerto Rico Electric Power Authority has established a maximum allowable ramp rate of 10% per minute of rated power [9]; a similar 10% of rated power on timescales within a dispatch period for active power rate limit is also recommended for generating plants in South Australia [10]; Ireland's EirGrid and Hawaiian Electric Company limit positive ramps to 30 MW min^{-1} [11] and 2 MW min^{-1} [12] respectively. Electrochemical energy storage devices (ESDs) integrated in PV systems provide a possible means of meeting these requirements by smoothing the PV power

* Corresponding author.
E-mail address: p.burr@unsw.edu.au (P.A. Burr).

https://doi.org/10.1016/j.jpowsour.2019.03.055
Received 11 December 2018; Received in revised form 27 February 2019; Accepted 15 March 2019
Available online 25 March 2019
0378-7753/

Acronyms

ESD	Energy Storage Device
MPPT	Maximum Power Point Tracking
SoC	State of Charge

Nomenclature

C_{DC}	inverter DC link capacitance
$C_{ESD,i}$	single module-based capacitive energy storage device
C_{ESD}	total module-based capacitive energy storage capacitance
$C_{PV,i}$	single PV module internal capacitance
$D_{bp,i}$	bypass diode
$E_{ESD,i}$	single module-based capacitive energy storage device rated energy
E_{ESD}	total module-based capacitive energy storage device rated energy
E_{ESDnom}	total energy stored in energy storage device at nominal voltage
I_{CS1}	current generated by first current source
I_{CS2}	current generated by second current source
I_{DC}	current fed into inverter
I_{max}	maximum allowable current
I_{SC0}	PV module short circuit current
K_P	proportional controller parameter
P_{DC}	power fed into inverter
P_{ESD}	total capacitive energy storage power
P_{GRID}	grid power
$P_{PV,i}$	single PV module generated power
P_{PV}	total PV module generated power
$P_{PVrated}$	total PV module rated power
P_{res}	restoring power
RR_{GRID}	grid power ramp rate
RR_{limit}	ramp rate limit
RR_{PV}	PV power ramp rate
$RR_{PV\text{-}GRID}$	PV-grid power ramp rate
RR_{res}	restoring power ramp rate
V_{DC}	inverter DC link voltage
V_{DC}^{*}	inverter DC link reference voltage
V_{DCmax}	inverter DC link maximum voltage
V_{DCmin}	inverter DC link minimum voltage
V_{DCnom}	inverter DC link nominal voltage
$V_{ESD,i}$	single module-based capacitive energy storage voltage
V_{ESD}	total module-based capacitive energy storage voltage

output at the source [13]. In addition, distributed energy storage systems may offer ancillary services such as voltage and frequency control to support the grid [14].

Our recent report [13] evaluated a set of representative electrochemical energy storage technologies (including high-power batteries, high-energy batteries, electrochemical capacitors and electrolytic capacitors) for power ramp rate control of PV systems with large (7.2 MW), small (100 kW), array-level (5 kW) and module-level (280 W) capacity. Electrochemical capacitors have higher increased cycle life (typically more than 10^6 cycles) compared to rechargeable batteries, higher power densities and lower discharge rates [15]. However, their relatively low energy densities make them less applicable to integration at a system level in large PV installations but more suitable for PV module-level integration, since integration at an array level and in larger PV installations would require an impractical number of capacitors to satisfy the energy requirement. Meanwhile, module-level ramp rate control offers several advantages, such as increased system reliability, monitoring functionality, which are useful for minimizing partial shading effects and thereby enhancing system efficiency, and allowing module mismatches and combinations of different module orientations [16,17]. Despite that, it is unclear whether these module-level systems employing electrochemical capacitors would require more complex control schemes.

The integration of control schemes for ESDs and inverters is an obstacle to overcome for power smoothing in PV systems [18], and different control methods were studied to solve the power fluctuation problems. It has been proposed that low pass filters can be used to attenuate the high-frequency components of the delivered power and reduce power fluctuations by determining the smoothed power reference and generating commands to control the ESDs [19–21], but implementations of low pass filters do not strictly constrain the power variations within grid regulation limits. Moving average methods (traditional [22], exponential [23], Euler-type [24]) have also been implemented to smooth the output fluctuations as the control target for the PV system. However, moving average-based control methods cannot reflect future output with historical data or control the ramp rate directly, and they require a memory device to store the long averaging window. Therefore, in the current study, the target output for ramp rate requirement was determined directly by calculating and comparing PV power and the required output power at each timestep, as reported in recent studies [25–27]. Ramp rate control can be also realized through active power curtailment by modifying the inherent maximum power point tracking (MPPT) algorithm [28,29]. Previous studies have focused on improving the MPPT algorithm for a single PV module [28,29], the use of energy storage for large-scale PV systems [30–33], as well as some hybrid energy storage systems, such as fuel cell [34], hydrogen [35] and batteries [36–41], however few considered the potential of PV module-based energy storage.

The main contribution of this paper is a novel control approach that utilizes module-based capacitive energy storage to control the ramp rate of the power injected by an array of PV modules into the AC grid. With the assumption that technology advances sufficiently for the size and cost of the required ESDs to be reasonable, our case study shows that under the proposed control, the generation power ramp rate compliance of PV arrays can be improved dramatically with the use of capacitive ESDs installed at the module level of series-connected PV modules. Since the utilization of energy stored in electrochemical capacitors is not only related to their capacitance, but also their operating voltage window, this study introduces a new parameter describing an acceptable voltage margin of inverter DC link voltage, and further discusses the control for the charge and discharge operations hence ramp rate of a capacitive storage system by varying the controllable reference voltage of the inverter DC link. In turn, the reference voltage is calculated from the power and energy requirements of the electrochemical capacitors to meet ramp rate restrictions and constraints. The proposed control methods are tested through extensive simulations based on 1-s irradiance data obtained from a rooftop weather station located at UNSW Sydney, Australia.

The paper is organized as follows. In Section 2, an equivalent circuit model for a single-phase grid-connected module-based PV system is proposed, and a novel ramp rate control scheme for PV systems is presented in Section 3. Section 4 compares modelling results with respect to different ramp rate controls, energy storage sizes and acceptable voltage margin to verify the proposed model and control schemes, and conclusions are drawn in Section 5.

2. Model of photovoltaic systems

An equivalent circuit diagram for a single-phase grid-connected PV system with module-integrated DC-DC optimizers and an inverter is

shown in Fig. 1(a). A module-integrated DC-DC optimizer (typically a non-inverting buck-boost converter [42]) maximizes the power from each PV module individually and decouples the MPPT control from the grid side control [43]. With the dedicated optimizers connected to a common central or string DC-AC inverter, the inverter is used to maintain an acceptable DC link voltage and control the grid current. The variable $C_{PV,i}$ represents the relatively small internal capacitance of each PV module, and $C_{ESD,i}$ represents the module-based capacitive energy storage. The voltage across each capacitor $V_{ESD,i}$ shares the DC input voltage of the inverter V_{DC}. The DC link capacitor, C_{DC}, is typically thousands of microFarads and filters the ripple voltage on the DC link. The bypass diode $D_{bp,i}$ is integrated with the module to eliminate high reverse voltages during shading events. If all PV modules in a series-connected array output the same power $P_{PV,i}$, the single-phase grid-connected PV system in Fig. 1(a) can be modelled with average-value modelling techniques [44], using the equivalent circuit model proposed in Fig. 1(b) to characterize the dynamics of series-connected PV modules with their module-integrated DC-DC optimizers and inverter for system-level analysis.

The current source CS1 in Fig. 1(b) represents the series-connected PV modules with their module-integrated DC-DC optimizers, and its current, I_{CS1}, defined as:

$$I_{CS1} = \min\left(\frac{P_{PV}}{V_{DC}}, I_{max}\right) \tag{1}$$

where

$$P_{PV} = \sum_{i}^{n} P_{PV,i} = nP_{PV,i} \tag{2}$$

P_{PV} is the total power generated by the PV array, and I_{max} is the maximum allowable current in the circuit, which is usually taken as the value of short circuit current I_{SC0} of the PV modules. Therefore, the value of current source CS1 is limited to the range:

$$0 \le I_{CS1} \le I_{SC0} \tag{3}$$

The current source CS2 in Fig. 1(b) represents the power delivered to the AC grid via the DC link:

$$I_{CS2} = K_P(V^*_{DC} - V_{DC}) \tag{4}$$

where

$$V_{DC} = \sum_{i}^{n} V_{ESD,i} \tag{5}$$

and the current source CS2 uses a proportional controller to regulate the DC link voltage fixed at the reference voltage V^*_{DC} [45]. The comprehensive analysis of topology and control for the grid-connected inverter is not within the scope of this paper, and more details can be found in [46–48]. The DC link voltage, V_{DC}, is the same as the total voltage across the series capacitors, and K_P is the proportional controller parameter. The equivalent capacitance, C_{ESD}, for the series string of capacitors (denoted by $C_{ESD,i}$) is equal to $C_{ESD,i}/n$, with n being the number of PV modules, and rated energy $E_{ESD,i}$ is stored in the module-based capacitor $C_{ESD,i}$, which is further discussed in Section 4.

For our case study, the PV specifications were chosen to match those of a system consisting of Trina HONEY TSM-PD05 60–280 PV modules [49], and the modelling parameters are listed in Table 1. The voltage at the maximum power point is taken as the nominal voltage of each capacitor link, and the corresponding maximum power is assumed to be the PV rated power for each module in Fig. 1(a). To obtain the maximum power, each module-integrated DC-DC optimizer tracks the MPP of the connected PV module, and the inverter controls the DC link voltage by adapting the current I_{DC}, where the proportional controller parameter K_P equal to $10/n$ is chosen.

It is assumed that the inverter regulates the AC current in phase with the voltage such that the power factor is unity. For simplicity, the current in the comparatively small DC link capacitor is ignored, and the voltages across all the components are the same. Without considering power losses (e.g., semiconductor switching/conduction, inefficiencies in the ESDs, transmission lines), the power at the PV source P_{PV}, capacitive energy storage device P_{ESD} and inverter P_{DC} can be represented as:

$$P_{PV} = I_{CS1}V_{DC} \tag{6}$$

$$P_{ESD} = I_{ESD}V_{DC} = \left(C_{ESD}\frac{dV_{DC}}{dt}\right)V_{DC} = C_{ESD}V_{DC}\dot{V}_{DC} \tag{7}$$

$$P_{DC} = I_{DC}V_{DC} \tag{8}$$

In this paper, the reference voltage V^*_{DC} (see Eq. (4)) is not a constant but a controlled variable, determined from the required power and energy for the capacitor C_{ESD}, which aims to meet the PV generation ramp rate requirements by utilizing the energy stored in the capacitor. The power fed into inverter P_{DC} is equivalent to the power delivered to the grid P_{GRID}, which in turn is determined by the proposed ramp rate control scheme that is discussed in Section 3.

3. Ramp rate control scheme

In order to compensate for the PV power excursions, the capacitor should be charged and discharged at a certain rate to meet the ramp rate requirements, and the difference between the actual PV power $P_{PV}(t)$ and the power delivered to the grid $P_{GRID}(t)$ defines the power exchanged with the capacitor $P_{ESD}(t)$:

$$P_{ESD}(t) = P_{PV}(t) - P_{GRID}(t) \tag{9}$$

When the PV power is larger than the power delivered to the grid, $P_{ESD}(t)$ is positive and the capacitor is charged to store the excess energy from the PV module in order to remain within the positive ramp rate limit. When the PV power is smaller than the grid power, $P_{ESD}(t)$ is negative and the capacitor is supplying energy to the grid to limit the negative ramp rate. The change of energy stored in the capacitor at the time instant t, $\Delta E_{ESD}(t)$, is expressed as a function of the capacitor

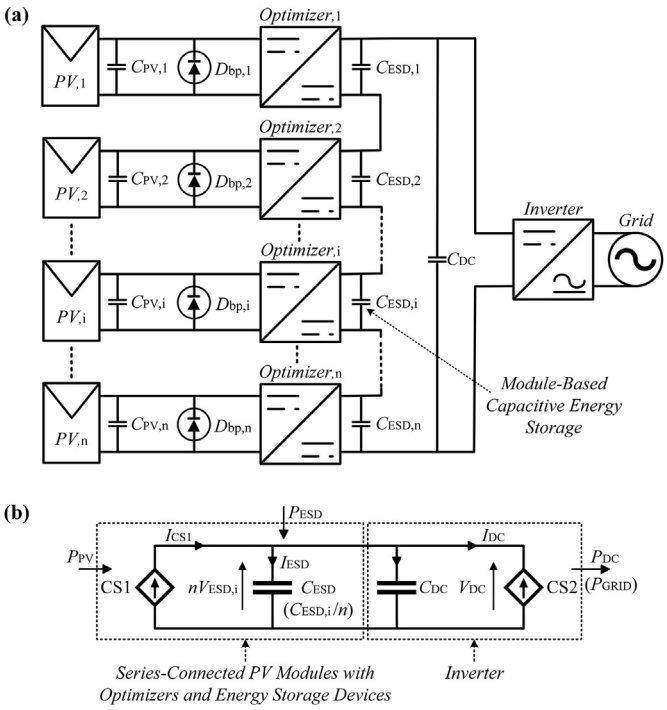

Fig. 1. (a) Single-phase grid-connected PV system with module-integrated DC-DC optimizers, inverter and module-based capacitive energy storage $C_{ESD,i}$. (b) Proposed equivalent circuit model for a single-phase grid-connected PV system.

Table 1
Modelling parameters and values used for the model.

Parameter	Value
Power at maximum power point of PV module	280 W
Voltage at maximum power point of PV module	31.4 V
Current at maximum power point of PV module	8.92 A
Short circuit current of PV module (I_{SC0})	9.4 A
Proportional controller (K_P)	10/*n*

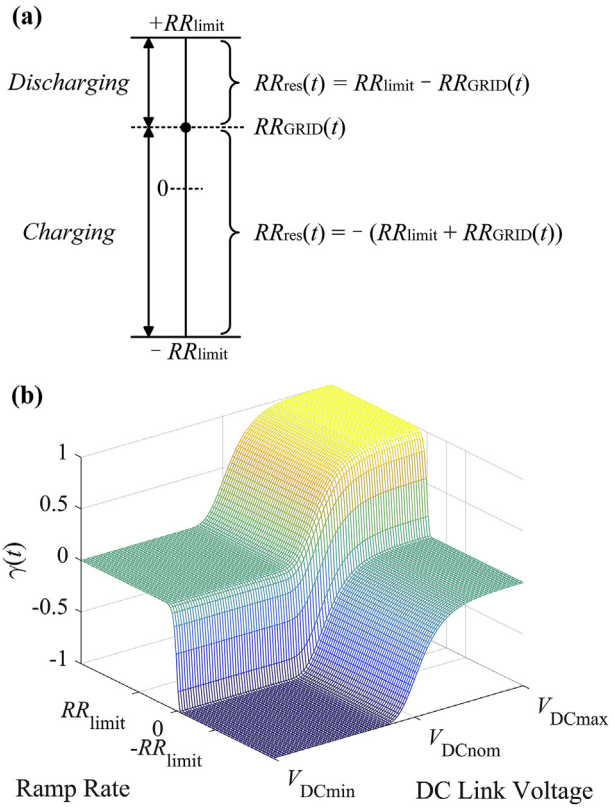

Fig. 2. (a) Relation between RR_{limit}, $RR_{GRID}(t)$ and $RR_{res}(t)$ at an instant *t*. (b) 3D plot for $\gamma(t)$ as a function of inverter DC link reference voltage $V^*_{DC}(t-\Delta t)$ and ramp rate $RR_{PV\text{-}GRID}(t)$, where $b_1 = 10$, $b_2 = 30$.

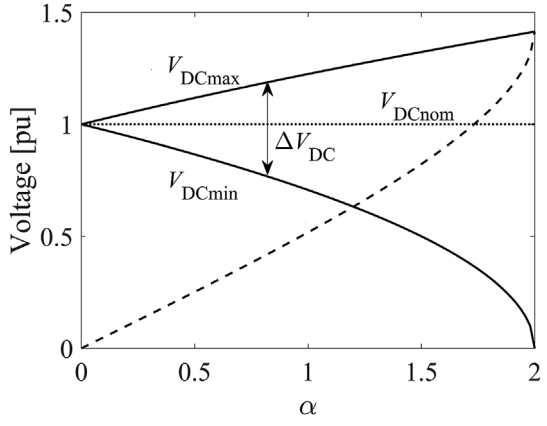

Fig. 3. Variation of nominal voltage V_{DCnom}, maximum voltage V_{DCmax}, minimum voltage V_{DCmin}, and difference between maximum and minimum voltage ΔV_{DC} (dashed curve) with α.

instantaneous power $P_{ESD}(t)$,

$$\Delta E_{ESD}(t) = E_{ESD}(t) - E_{ESD}(t-\Delta t) = \int_{t-\Delta t}^{t} P_{ESD}(t)\,dt \tag{10}$$

Consequently, the variable inverter DC link reference voltage $V^*_{DC}(t)$ can be derived based on the required capacitor compensation energy,

$$V^*_{DC}(t) = \sqrt{V^{*2}_{DC}(t-\Delta t) + \frac{2[E_{ESD}(t) - E_{ESD}(t-\Delta t)]}{C_{ESD}}} \tag{11}$$

To calculate the required capacitor power $P_{ESD}(t)$ in Eq. (9), as well as the corresponding required capacitor energy change $\Delta E_{ESD}(t)$ in Eq. (10) and the reference voltage $V^*_{DC}(t)$ in Eq. (11), the power exported to the grid for a given set of ramp rate limitations should be determined first. Previous work considered simple ramp rate control implementations [22] to limit the grid power to the acceptable ramp rate limits (see Fig. S1, Supporting Information). However, within this control scheme, no effort is made to restore the capacitor's state of charge (SoC) back to its optimum when the PV power is within the limits. Therefore, a novel ramp rate control scheme is proposed, named SoC-optimized control scheme, which optimizes the capacitor's state of charge while restricting the PV power generation within ramp rate requirements.

In both the simple and the SoC-optimized control schemes, the relevant ramp rate to be compared against regulatory limitations (RR_{limit}) is the parameter $RR_{PV\text{-}GRID}(t)$, as defined in Eq. (12), which compares the PV power at the current timestep, $P_{PV}(t)$, to the grid power at the previous timestep, $P_{GRID}\ (t-\Delta t)$,

$$RR_{PV-GRID}(t) = \frac{P_{PV}(t) - P_{GRID}(t-\Delta t)}{P_{PVrated}\Delta t} \tag{12}$$

where $P_{PVrated}$ is the rated PV power (equivalent definitions of parameters $RR_{PV}(t)$ and $RR_{GRID}(t)$ are provided in Supporting Information). When the PV power is within the limits, additional power can be exchanged with the capacitor to be further charged or discharged to rebalance the DC link voltage (SoC of the capacitor) but with the constraint that the additional power exchange must not lead to a violation of the ramp rate limits. This additional power change for the grid is termed the restoring power, notated $\Delta P_{res}(t)$,

$$\Delta P_{res}(t) = RR_{res}(t) P_{PVrated}\Delta t \tag{13}$$

where $RR_{res}(t)$ is the ramp rate increment to the additional power change. For instance, when $V^*_{DC}(t)$ is lower/higher than V_{DCnom}, the capacitor can be further charged/discharged towards the nominal DC link voltage with the additional power $\Delta P_{res}(t)$. To ensure that the additional power change in the grid does not violate the ramp rates, the following relation between RR_{limit}, $RR_{GRID}(t)$ and $RR_{res}(t)$, must be guaranteed to ensure that the total ramp rate is within limits,

$$|RR_{GRID}(t) + RR_{res}(t)| \le RR_{limit} \tag{14}$$

where a positive $RR_{GRID}(t)$ scenario is illustrated in Fig. 2(a). Thus, a novel ramp rate control algorithm is proposed as follows: the power delivered to the grid is modified as:

$$P_{GRID}(t) = P_{GRID}(t-\Delta t) + \gamma(t)\Delta P_{GRIDmax} \tag{15}$$

where

$$\Delta P_{GRIDmax} = P_{PVrated} RR_{limit}\Delta t \tag{16}$$

and the parameter $\gamma(t)$ represents the portion (between [–1, 1]) of allowable grid power change, which is a function of both $V^*_{DC}(t-\Delta t)$ and $RR_{PV\text{-}GRID}(t)$:

$$\gamma(t) = \exp(-\exp(-b_1(V^*_{DC}(t-\Delta t)/V_{DCnom} - 1))) + \exp(-\exp(-b_2(RR_{PV-GRID}(t)/RR_{limit}))) - 1 \tag{17}$$

Here, we use a linear combination of two sigmoidal Gompertz functions to describe the $V^*_{DC}(t-\Delta t)$ and $RR_{PV\text{-}GRID}(t)$ dependency of $\gamma(t)$, as illustrated in Fig. 2(b), where the inflection points of $\gamma(t)$ are

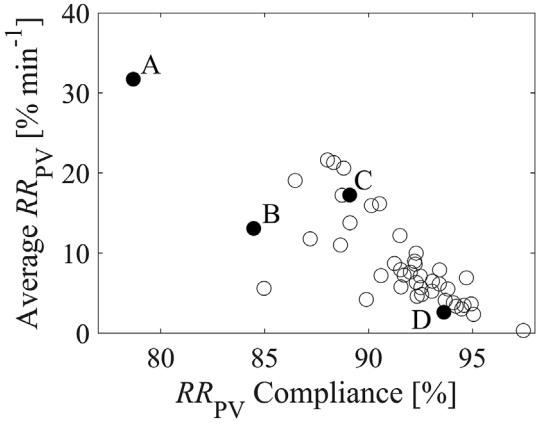

Fig. 4. PV power ramp rate characteristics of the 46-day dataset in terms of daily ramp rate compliance and daily ramp rate average.

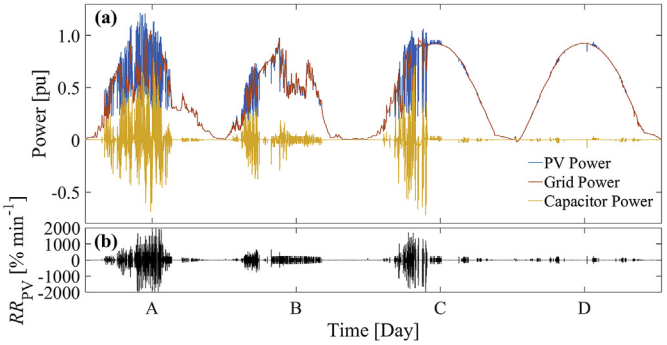

Fig. 5. (a) PV power, the determined power delivered to grid and the required capacitor power for each PV module with integrated module-based capacitive energy storage, which are based on the irradiance data with 1-s resolution during the four chosen days from UNSW Kensington campus, Sydney, Australia, where power is normalized by PV module rated power, i.e., 280 W. (b) Corresponding PV generation ramp rate.

Table 2
Different module-based capacitive energy storage devices used for ramp rate performance comparison in Fig. 6.

Subplot	System Parameter			
(a) (b)	C_{ESD} (F)		22.7	
	α		1.0	
	V_{ESDmax} (V)		38.5	
	E_{ESD} (puE)		1.0	
(c)		α = 1.0		
	C_{ESD} (F)	45.4	68.1	90.8
	V_{ESDmax} (V)	38.5	38.5	38.5
	E_{ESD} (puE)	2.0	3.0	4.0
(d)		C_{ESD} = 22.7 F		
	α	0.2	0.5	1.5
	V_{ESDmax} (V)	32.9	35.1	41.5
	E_{ESD} (puE)	0.2	0.5	1.5
(e)		E_{ESD} = 1.0 puE		
	C_{ESD} (F)	31.0	27.3	19.5
	α	0.2	0.5	1.5
	V_{ESDmax} (V)	32.9	35.1	41.5

located at V_{DCnom} and zero along voltage and ramp rate direction respectively. The parameters b_1 and b_2 control the rate of change at the inflection points, and the sensitivity to the choice of parameters b_1 and b_2 is discussed in the following section. By having a linear combination of two orthogonal functions, we can control the balance between supply (available voltage margin) and demand (ramp rate requirement) of restoring power, whilst ensuring continuous and smooth transitions at all values of voltage and ramp rate. Avoiding discontinuities in [V^*_{DC}, $RR_{PV\text{-}GRID}$] space is paramount, as these lead to instabilities when transitioning from one operational mode to another (e.g., one mode in which the voltage below the nominal V_{DCnom} and ramp rate beyond the limit RR_{limit}, and another mode in which the voltage below the nominal but ramp rate within the limits).

With the proposed control scheme, the power exchange within the capacitors is determined not only by the ramp rate $RR_{PV\text{-}GRID}(t)$, but also the DC link reference voltage $V^*_{DC}(t)$, indicating that the capacitors must have freedom to charge and discharge as required. This is achieved by allowing the voltage to vary across a specified voltage window. By defining a maximum and minimum DC operating voltage, V_{DCmax} and V_{DCmin} respectively, a parameter α is introduced here to represent the magnitude of the voltage window in terms of the energy stored,

$$\alpha = \frac{\Delta E_{ESDmax}}{E_{ESDnom}} = \frac{\frac{1}{2}C_{ESD}(V^2_{DCmax} - V^2_{DCmin})}{\frac{1}{2}C_{ESD}V^2_{DCnom}} = \frac{V^2_{DCmax} - V^2_{DCmin}}{V^2_{DCnom}} \quad (18)$$

where E_{ESDnom} is the energy stored in a capacitor at the nominal voltage V_{DCnom} of the DC link, and ΔE_{ESDmax} represents the maximum available energy in the capacitor for ramp rate compensation. The operating voltage limits for a given nominal voltage V_{DCnom} and α are (see Supporting Information for detailed derivations):

$$V_{DCmax} = \sqrt{\frac{2+\alpha}{2}}V_{DCnom} \quad (19)$$

$$V_{DCmin} = \sqrt{\frac{2-\alpha}{2}}V_{DCnom} \quad (20)$$

where the maximum voltage V_{DCmax} also represents the required rated voltage for capacitor. Fig. 3 implies that the inverter DC link voltage is allowed to vary across an acceptable range [V_{DCmin}, V_{DCmax}] to charge or discharge the capacitor. When the determined reference voltage $V^*_{DC}(t)$ is beyond the acceptable limits, the reference voltage is set to the corresponding minimum or maximum voltage respectively. The determination of parameter α has a direct impact on ramp rates, such as compliance and average, and the method of determining an effective value for α is discussed with modelling results in Section 4.

4. Results

4.1. Performance of simple and SoC-optimized ramp rate control schemes

Irradiance data with 1-s resolution was obtained from UNSW Kensington campus, Sydney, Australia over a 46-day period from 12 December 2015 to 23 May 2016, as published previously [13]. The characteristics of this dataset in terms of daily ramp rate compliance (i.e., the fraction of 1-s instances in which the ramp rate was within typical regulatory limits of 10% min^{-1} [13]) and daily ramp rate average are depicted in Fig. 4. Four representative days with distinctly different characteristics are labelled A, B, C and D. Fig. 5(a) shows, for the representative days, the PV power without ramp rate control scheme (blue, refer to [13] for detailed calculations), the calculated power delivered to the grid (red) and the required capacitor power for each PV module (yellow), and Fig. 5(b) depicts the corresponding instantaneous ramp rate.

To simplify the comparisons for ramp rate performance between different sizes of module-based capacitive ESDs, the module-based capacitive ESD rated energy E_{ESD} (i.e., the amount of energy stored in a capacitor C_{ESD} at the rated voltage V_{ESDmax}) is represented in per-unit energy (puE),

$$E_{ESD} = \frac{1}{2}C_{ESD}V^2_{ESDmax} = \frac{2+\alpha}{4}C_{ESD}V^2_{ESDnom} \quad (21)$$

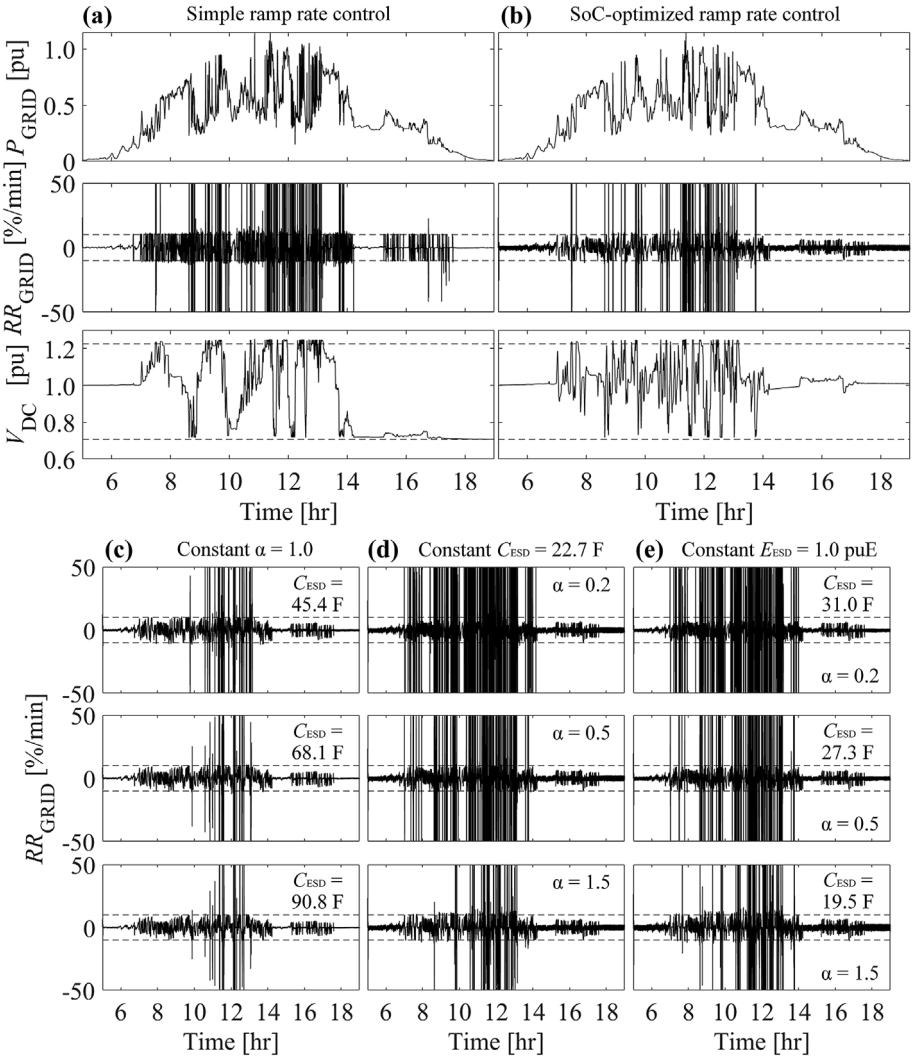

Fig. 6. Grid power, ramp rate and DC link voltage with module-based capacitive ESD capacitance C_{ESD} = 22.7 F and α = 1.0 under (a) simple ramp rate control and (b) SoC-optimized ramp rate control. The RR_{GRID} compliance and average are 85.5% and 12.9% min^{-1} in (a) and 94.4% and 8.5% min^{-1} in (b). Grid power ramp rate comparisons under the proposed control between (c) different capacitance C_{ESD} for the same α = 1.0, (d) different α for the same C_{ESD} = 22.7 F, and (e) different combinations of C_{ESD} and α for the same E_{ESD} = 1.0 puE, with a decrease in C_{ESD} accompanied by an increase in α.

where notations C_{ESD}, V_{ESDmax} and E_{ESD} are used to simplify the representations of module-based capacitors assuming that n is equal to 1 in Section 2. Therefore, the base quantity for module-based capacitive ESD rated energy is equal to 16.8 kJ puE^{-1} (~4.67 W h puE^{-1}) for each 280 W PV module, and 1.0 puE module-based capacitive ESD rated energy E_{ESD} approximately corresponds to the energy stored in a 22.7 F electrochemical capacitor at the rated voltage of 38.5 V (i.e., nominal voltage of 31.4 V and α = 1.0).

In the following analysis, we used values of C_{ESD} and α listed in Table 2 and parameters b_1^* = 20.6 and b_2^* = 68.4, which were obtained through an optimization strategy described in Section 4.3 together with a detailed analysis of the sensitivity of the results to these parameters. Fig. 6(a–b) show the output power, the ramp rate and the DC link voltage for the most variable day in our dataset (Day A) under the simple control scheme (a) [22] and the proposed SoC-optimized ramp rate control scheme (b), respectively. The dashed lines represent the assumed regulatory limits for ramp rate (±10% min^{-1}) and acceptable voltage range (V_{DCmax} and V_{DCmin}) respectively.

When the DC link voltage was above/below the nominal value, the proposed SoC-optimized scheme returned the DC link voltage back to nominal much faster than the simple control scheme by exporting/importing power to/from the grid. This means that the capacitor was at its near-optimal SoC (V_{ESD} = V_{ESDnom}) and ready for the next rapid PV power fluctuation. The ramp rate compliances were 94.4%, 85.5% and 77.9% with the proposed SoC-optimized ramp rate control, simple ramp rate control and no ramp rate control respectively, and the corresponding average ramp rates were 8.5% min^{-1}, 12.9% min^{-1} and 31.7% min^{-1}.

Under the proposed ramp rate control scheme, the output power ramp rate was compared for different module-based capacitive ESD capacitance C_{ESD} in Fig. 6(c) and parameter α in Fig. 6(d) to observe their effects on ramp rate. Compared with the ramp rate of PV generation without an ESD (which attained instantaneous values of nearly 2000% min^{-1}, see Fig. 5(b)), it is clear that the ramp rates were significantly reduced by increasing the capacitance C_{ESD} for a given α (1.0). Comparisons in Fig. 6(d) show that, with the increase of acceptable voltage range (α increased from 0.2 to 1.5), the ramp rates were also reduced for a given capacitance C_{ESD} (22.7 F). Since the allowable DC link voltage window was dictated by α, when α was small (e.g., 0.2), the DC link voltage often reached the limit, indicating that the capacitor could not be charged/discharged any further, and the usable energy within the capacitor was limited by the rated voltage V_{ESDmax}. This situation resulted in ramp rates that exceeded the acceptable limits. With a larger α, for example when α was set to 1.5, the larger voltage range

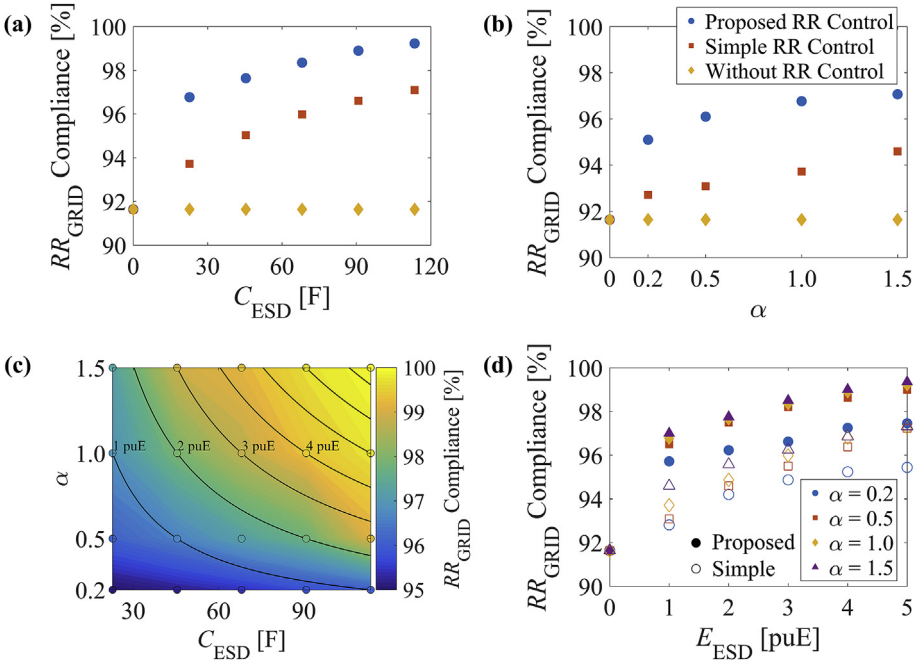

Fig. 7. Comparisons of ramp rate compliance based on 46-day data between different control schemes with respect to (a) capacitance C_{ESD} for the same $\alpha = 1.0$ and (b) inverter DC link voltage window α for the same $C_{ESD} = 22.7$ F. (c) Effect of changing both C_{ESD} and α on RR_{GRID} compliance under the proposed SoC-optimized ramp rate control, where the labels represent total stored energy in puE. (d) Ramp rate compliance for different combinations of C_{ESD} and α for five given ESD rated energy E_{ESD} values.

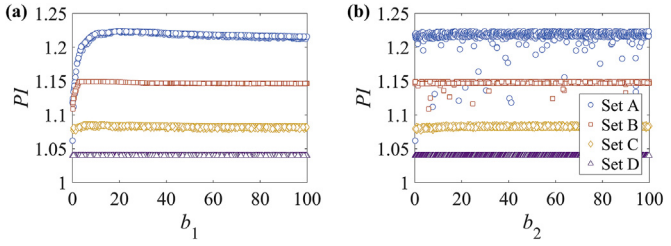

Fig. 8. Comparisons of performance index *PI* with respect to (a) parameter b_1 and (b) parameter b_2 between Day A, B, C, D with $C_{ESD} = 22.7$ F and $\alpha = 1.0$.

Table 3
Optimal parameters for four chosen days.

Day	A	B	C	D
b_1^*	20.6 ± 1.0	12.2 ± 0.4	7.0 ± 2.4	2.3 ± 1.5
b_2^*	68.4 ± 11.7	59.6 ± 24.2	67.9 ± 21.6	89.4 ± 10.2

allowed the DC link voltage to be varied without reaching the voltage limits even for the module-based capacitive ESDs with lower capacitance, thus reducing the instances where the ramp rate could not be controlled within the acceptable limits. However, on the most variable irradiance day (Day A, as shown in Fig. 5), increasing α (V_{ESDmax}) was not sufficient to achieve 100% ramp rate compliance, and ESDs with higher capacitance (C_{ESD}) were required.

Fig. 6(e) presents the grid power ramp rate for three combinations of C_{ESD} and α values that resulted in 1.0 puE of E_{ESD}. For a fixed energy storage quanta, a reduced average ramp rate (7.2% min^{-1}) and an increased ramp rate compliance (94.8%) were achieved using smaller capacitances with higher voltage range ($C_{ESD} = 19.5$ F, $\alpha = 1.5$). This implies that under the proposed control scheme, for the same amount of rated energy E_{ESD}, the choice of smaller capacitance C_{ESD} with higher rated voltage V_{ESDmax} could be more beneficial for grid power ramp rate performance.

4.2. Statistical analysis of ramp rate control schemes

The performance of different ramp rate control schemes was further evaluated using the full 46-day dataset. The average power ramp rate compliance of the 46 days without any ESDs and ramp rate control schemes was 91.6%, which should be considered the benchmark value. This value was dramatically improved to 96.8% by adding 22.7 F electrochemical capacitors at the rated voltage of 38.5 V ($\alpha = 1.0$) at the PV module level. For the same size of capacitance C_{ESD}, the simple control scheme achieved a comparatively small increase in ramp rate compliance (93.7%). The proposed control scheme yielded a higher compliance for any given capacitance C_{ESD} (Fig. 7(a)) and voltage window α (Fig. 7(b)), highlighting that maintaining the capacitor's SoC closer to the optimal value enabled it to respond to PV fluctuations on more occasions and hence more effectively control the ramp rate within regulatory limits. It must be noted that the improved ramp rate compliance with the SoC-optimized control came at no additional hardware cost.

The relationship between module-based capacitive ESD capacitance (C_{ESD}), operating voltage window (α) and the resulting grid power ramp rate compliance under the SoC-optimized control scheme is shown in Fig. 7(c). Clearly, an increase in ramp rate compliance could be achieved either by increasing the capacitance or by increasing the voltage window. Thus, a given ramp rate compliance may be achieved with different combinations of C_{ESD} and α. Similar to what is shown in Fig. 6(e), for a given amount of rated energy E_{ESD}, such as 1.0 puE, 2.0 puE and 3.0 puE depicted in Fig. 7(c), an improved ramp rate compliance can be achieved by using a larger voltage window. Fig. 7(d) compares grid power ramp rate compliance between different control schemes for different rated energy E_{ESD}. For the same rated energy E_{ESD}, increasing the voltage window (α) led to a relatively larger increase in ramp rate compliance compared to increasing capacitance C_{ESD}. Specifically, it is suggested that cost-effective solutions would require α larger than 0.2.

4.3. Sensitivity analysis of control scheme to choice of parameters

The proposed SoC-optimized control scheme depends on two parameters, b_1 and b_2, as per Eq. (17). Here we investigated the performance of the control scheme when these parameters were chosen differently, and proposed a robust method for the choice of parameters for any arbitrary PV system and location. These parameters were optimized by iteratively performing simulations on a one-day training dataset (Day A of Fig. 5) and varying b_1 and b_2 until maximal a grid power ramp rate compliance value was reached. Specifically, we monitored a performance index:

$$PI = \frac{n(|RR_{GRID}(t)| \leq RR_{limit})}{n(|RR_{PV}(t)| \leq RR_{limit})} \quad (22)$$

where n was the number of occurrences. The performance index PI was a measure of the improvement in RR_{GRID} compliance compared to the benchmark PV power (without ESDs and control schemes), thus a higher value implied a more effective scheme whilst a value of 1 meant no improvement.

Maintaining the same module-based capacitive ESD capacitance ($C_{ESD} = 22.7$ F) and voltage window ($\alpha = 1.0$), a sensitivity analysis was performed by repeating the optimization for four days with distinctly different PV power ramp rate characteristics, as depicted in Fig. 5. Fig. 8(a–b) show, for each of the four days, the performance index variation with b_1 and b_2 for 1000 generated points, uniformly distributed in the range between 0 and 100. As expected, the days with high variability benefitted the most (high performance index) compared to low-variability days. It is also evident that for days with low variability, the method was largely unaffected by the choice of parameters and the maximum RR_{GRID} compliance was reached for all values. For highly variable days, the scheme was sensitive to b_1 but still largely insensitive to b_2. An insufficiently small value of b_1 (insufficiently steep gradient of $\gamma(t)$ with respect to voltage) led to an ineffective control scheme, but too large a value did not lead to significant inefficacy. This provides a simple means for a conservative choice of values if training the values using irradiance data from a highly variable day was not possible: large b_1 ($\sim$20) coupled with any reasonable value of b_2 (1–100). Table 3 shows the average of the best-performing 1% of solutions (10 pairs) together with their standard deviation to characterize the breadth of the optima, which is clearly very broad for b_2 but narrower for b_1 in highly variable conditions.

5. Conclusion and outlook

A solution for controlling the generation ramp rates of PV systems in electrical grids using PV module-based capacitive energy storage devices and a novel ramp rate control algorithm were proposed. The acceptable voltage margin and voltage control methods for the inverter DC link were investigated to enable the charging and discharging operations of capacitors to limit ramp rates of an array of series-connected PV modules. With the measured 1-s irradiance data obtained from a rooftop weather station located at UNSW Sydney, Australia, we show that for a highly variable day, the power ramp rate compliance of a PV system with series-connected 280 W PV modules can be increased from 77.9% to 94.8% using 19.5 F module-based energy storage devices rated at 41.5 V (equivalent to 16.8 kJ of energy storage) under the proposed SoC-optimized control scheme. Using the full 46-day dataset with 1-s resolution, the improvement in compliance was demonstrated over a representative period and for a range of energy storage sizes and voltage windows. For the same amount of rated energy, the choice of module-based capacitive energy storage devices with smaller capacitance and higher rated voltage could be more beneficial for improving generation ramp rates of PV systems. Sensitivity analyses with respect to training dataset and ramp rate control parameters suggested that the control scheme was largely insensitive to the choice of the model parameters and thereby could operate robustly in the presence of variable irradiance conditions.

With the proposed ramp rate control method, capacitive energy storage elements help to deliver PV power ramp rates within the specifications of the grid code. Controlling ramp rates to relevant standards or codes also helps reduce long-term frequency perturbations, since the excursions in the intermittent PV power generation of individual generators are now better regulated and hence are easier to compensate using other generators and intermittent sources. The proposed method also has some influence on the voltage at the point of common coupling, and the improved frequency control can provide improved long-term control of voltage levels. At present, due to high capital costs, it is still a challenge for electrochemical capacitor technologies to meet the required energy storage economically. With more advanced control techniques for energy storage devices, the utilization of capacitors could be further improved, thereby reducing the cost and the size of the energy storage components in PV systems.

Data availability

The raw data required to reproduce these findings and the processed results data are available to download from https://doi.org/10.26190/5c8ed32da8e8f.

Acknowledgements

This work was supported by the Australian Research Council through Discovery Grant DP170103219 “Advanced Electrochemical Capacitors”. The authors would like to thank Dr. Mihai Ciobotaru for providing the solar irradiance data.

Appendix A. Supplementary data

Supplementary data to this article can be found online at https://doi.org/10.1016/j.jpowsour.2019.03.055.

References

[1] AEMO, South Australian Renewable Energy Report, (November 2017).
[2] R. Margolis, D. Feldman, D. Boff, Q4 2016/Q1 2017 Solar Industry Update, National Renewable Energy Lab (NREL), Golden, CO (United States), May 2017.
[3] H. Wirth, K. Schneider, Recent Facts about Photovoltaics in Germany, Report from Fraunhofer Institute for Solar Energy Systems, Germany, February 2018.
[4] X. Wu, et al., Stochastic optimal energy management of smart home with PEV energy storage, IEEE Trans. Smart Grid 9 (3) (2018) 2065–2075.
[5] B. Sivaneasan, et al., A new demand response algorithm for solar PV intermittency management, Appl. Energy 218 (2018) 36–45.
[6] P.G. McCormick, H. Suehrcke, The effect of intermittent solar radiation on the performance of PV systems, Sol. Energy 171 (2018) 667–674.
[7] N.K. Kandasamy, K.J. Tseng, S. Boon-Hee, Virtual storage capacity using demand response management to overcome intermittency of solar PV generation, IET Renew. Power Gener. 11 (2017) 1741–1748.
[8] S. Sayeef, et al., Solar Intermittency: Australia's Clean Energy Challenge. Characterising the Effect of High Penetration Solar Intermittency on Australian Electricity Networks, Australian Solar Institute (ASI), June 2012.
[9] V. Gevorgian, S. Booth, Review of PREPA Technical Requirements for Interconnecting Wind and Solar Generation, National Renewable Energy Lab (NREL), Golden, CO (United States), 2013.
[10] Australian Energy Market Operator (AEMO), Recommended Technical Standards for Generator Licensing in South Australia, (31 March 2017).
[11] EirGrid Grid Code, Version 6.0, (2015).
[12] A. Nelson, et al., Hawaiian Electric Advanced Inverter Grid Support Function Laboratory Validation and Analysis, National Renewable Energy Lab (NREL), 2016.
[13] Y. Jiang, et al., Suitability of representative electrochemical energy storage technologies for ramp-rate control of photovoltaic power, J. Power Sources 384 (2018) 396–407.
[14] M. Zeraati, G.M.E.H. olshan, J.M. Guerrero, Distributed control of battery energy storage systems for voltage regulation in distribution networks with high PV penetration, IEEE Trans. Smart Grid 9 (4) (2018) 3582–3593.
[15] P. Simon, Y. Gogotsi, Materials for electrochemical capacitors, Nature (2010) 320–329.
[16] S. Kouro, J. Leon, D. Vinnikov, L. Franquelo, Grid-connected photovoltaic systems: an overview of recent research and emerging PV converter technology, IEEE Ind. Electron. Mag. 9 (1) (2015) 47–61.
[17] F. Blaabjerg, Y. Yang, Overview of single-phase grid-connected photovoltaic

systems, Renewable Energy Devices and Systems with Simulations in MATLAB and ANSYS, CRC Press, 2017, pp. 41–66.
[18] T.D. Hund, S. Gonzalez, K. Barrett, Grid-tied PV system energy smoothing, 2010 35th IEEE Photovoltaic Specialists Conference, Honolulu, HI, 2010 002762-002766.
[19] G. Karmiris, T. Tengnér, Control method evaluation for battery energy storage system utilized in renewable smoothing, IECON 2013 - 39th Annual Conference of the IEEE Industrial Electronics Society, Vienna, 2013, pp. 1566–1570.
[20] K. Yoshimoto, T. Nanahara, G. Koshimizu, New control method for regulating state-of-charge of a battery in hybrid wind power/battery energy storage system, 2006 IEEE PES Power Systems Conference and Exposition, Atlanta, GA, 2006, pp. 1244–1251.
[21] S.K. Kim, J.H. Jeon, C.H. Cho, J.B. Ahn, S.H. Kwon, Dynamic modeling and control of a grid-connected hybrid generation system with versatile power transfer, IEEE Trans. Ind. Electron. 55 (4) (April 2008) 1677–1688.
[22] N. Kakimoto, H. Satoh, S. Takayama, K. Nakamura, Ramp-rate control of photovoltaic generator with electric double-layer capacitor, IEEE Trans. Energy Convers. 24 (2) (June 2009) 465–473.
[23] S.G. Tesfahunegn, Ø. Ulleberg, P.J. Vie, T.M. Undeland, PV fluctuation balancing using hydrogen storage–a smoothing method for integration of PV generation into the utility grid, Energy Procedia 12 (2011) 1015–1022.
[24] T. Monai, I. Takano, H. Nishikawa, Y. Sawada, A collaborative operation method between new energy-type dispersed power supply and EDLC, IEEE Trans. Energy Convers. 19 (3) (Sept. 2004) 590–598.
[25] M.J.E. Alam, K.M. Muttaqi, D. Sutanto, A novel approach for ramp-rate control of solar PV using energy storage to mitigate output fluctuations caused by cloud passing, IEEE Trans. Energy Convers. 29 (2) (June 2014) 507–518.
[26] X. Li, D. Hui, X. Lai, Battery energy storage station (BESS)-based smoothing control of photovoltaic (PV) and wind power generation fluctuations, IEEE Trans. Sustain. Energy 4 (2) (April 2013) 464–473.
[27] J. Marcos, O. Storkël, L. Marroyo, M. García, E. Lorenzo, Storage requirements for PV power ramp-rate control, Sol. Energy 99 (January 2014) 28–35.
[28] A. Sangwongwanich, Y. Yang, F. Blaabjerg, A cost-effective power ramp-rate control strategy for single-phase two-stage grid-connected photovoltaic systems, 2016 IEEE Energy Conversion Congress and Exposition (ECCE), Milwaukee, WI, 2016, pp. 1–7.
[29] R. Yan, T.K. Saha, Power ramp rate control for grid connected photovoltaic system, 2010 Conference Proceedings IPEC, Singapore, 2010, pp. 83–88.
[30] J. Marcos, I. de la Parra, M. García, L. Marroyo, Control strategies to smooth short-term power fluctuations in large photovoltaic plants using battery storage systems, Energies 7 (10) (2014) 6593–6619.
[31] I. De la Parra, et al., Control strategies to use the minimum energy storage requirement for PV power ramp-rate control, Sol. Energy 111 (2015) 332–343.
[32] R. van Haaren, M. Morjaria, V. Fthenakis, An energy storage algorithm for ramp rate control of utility scale PV (photovoltaics) plants, Energy 91 (2015) 894–902.
[33] S. Sukumar, H. Mokhlis, S. Mekhilef, M. Karimi, S. Raza, Ramp-rate control approach based on dynamic smoothing parameter to mitigate solar PV output fluctuations, Int. J. Electr. Power Energy Syst. 96 (2018) 296–305.
[34] P. Thounthong, et al., Energy management of fuel cell/solar cell/supercapacitor hybrid power source, J. Power Sources 196 (1) (2011) 313–324.
[35] Z. Huang, et al., Modeling and multi-objective optimization of a stand-alone PV-hydrogen-retired EV battery hybrid energy system, Energy Convers. Manag. 181 (2019) 80–92.
[36] H. Jia, Y. Mu, Y. Qi, A statistical model to determine the capacity of battery–supercapacitor hybrid energy storage system in autonomous microgrid, Int. J. Electr. Power Energy Syst. 54 (2014) 516–524.
[37] J. Li, M.A. Danzer, Optimal charge control strategies for stationary photovoltaic battery systems, J. Power Sources 258 (2014) 365–373.
[38] L. Chong, et al., An optimal control strategy for standalone PV system with Battery-Supercapacitor Hybrid Energy Storage System, J. Power Sources 331 (2016) 553–565.
[39] L. Chong, et al., An adaptive learning control strategy for standalone PV system with battery-supercapacitor hybrid energy storage system, J. Power Sources 394 (2018) 35–49.
[40] X. Wu, et al., Stochastic control of smart home energy management with plug-in electric vehicle battery energy storage and photovoltaic array, J. Power Sources 333 (2016) 203–212.
[41] X. Wu, et al., Optimal integration of a hybrid solar-battery power source into smart home nanogrid with plug-in electric vehicle, J. Power Sources 363 (2017) 277–283.
[42] L. Callegaro, M. Ciobotaru, D.J. Pagano, E. Turano, J.E. Fletcher, A simple smooth transition technique for the non-inverting buck-boost converter, IEEE Trans. Power Electron. 33 (6) (June 2018) 4906–4915.
[43] S. Kouro, J. Leon, D. Vinnikov, L. Franquelo, Grid-connected photovoltaic systems: an overview of recent research and emerging PV converter technology, IEEE Ind. Electron. Mag. 9 (1) (2015) 47–61.
[44] S. Chiniforoosh, et al., Definitions and applications of dynamic average models for analysis of power systems, IEEE Trans. Power Deliv. 25 (4) (2010) 2655–2669.
[45] M. Kasper, D. Bortis, J.W. Kolar, Classification and comparative evaluation of PV panel-integrated DC–DC converter concepts, IEEE Trans. Power Electron. 29 (5) (May 2014) 2511–2526.
[46] S.B. Kjaer, J.K. Pedersen, F. Blaabjerg, A review of single-phase grid-connected inverters for photovoltaic modules, IEEE Trans. Ind. Appl. 41 (5) (Sept.-Oct. 2005) 1292–1306.
[47] S. Jain, V. Agarwal, A single-stage grid connected inverter topology for solar PV systems with maximum power point tracking, IEEE Trans. Power Electron. 22 (5) (Sept. 2007) 1928–1940.
[48] R. Teodorescu, M. Liserre, P. Rodriguez, Grid Converters for Photovoltaic and Wind Power Systems, John Wiley & Sons, 2011.
[49] The Honey Framed 60-Cell Module, Trina Solar, (2017).